Inorg. Chem. **2008**, *47*, 9905−9918

X-ray Absorption Spectroscopy of Hemes and Hemeproteins in Solution: Multiple Scattering Analysis

Paola D'Angelo,[*,†] Andrea Lapi,[†,‡] Valentina Migliorati,[†] Alessandro Arcovito,[||] Maurizio Benfatto,[§] Otello Maria Roscioni,[†] Wolfram Meyer-Klaucke,[⊥] and Stefano Della-Longa[*,§,#]

Dipartimento di Chimica, Università di Roma "La Sapienza", P. le A. Moro 5, 00185 Rome, Italy, Istituto CNR di Metodologie Chimiche-IMC, Sezione Meccanismi di Reazione, Dipartimento di Chimica, Università di Roma "La Sapienza", P.le A. Moro 5, 00185 Rome, Italy, Laboratori Nazionali di Frascati, INFN CP13, 00044 Frascati, Italy, Istituto di Biochimica e Biochimica Clinica, Università Cattolica del Sacro Cuore, L.go F. Vito 1, 00168 Rome, Italy, European Molecular Biology Laboratory, Hamburg Unit, Deutsches Elektronen Synchrotron, Notkestrasse 85, D-22607 Hamburg, Germany, and Dipartimento di Medicina Sperimentale, Università dell'Aquila, Via Vetoio 67100, L'Aquila, Italy

Received May 29, 2008

A full quantitative analysis of Fe K-edge X-ray absorption spectra has been performed for hemes in two porphynato complexes, that is, iron(III) tetraphenylporphyrin chloride (Fe(III)TPPCl) and iron(III) tetraphenylporphyrin bis(imidazole) (Fe(III)TPP(Imid)$_2$), in two protein complexes whose X-ray structure is known at atomic resolution (1.0 Å), that is, ferrous deoxy-myoglobin (Fe(II)Mb) and ferric aquo-myoglobin (Fe(III)MbH$_2$O), and in ferric cyano-myoglobin (Fe(III)MbCN), whose X-ray structure is known at lower resolution (1.4 Å). The analysis has been performed via the multiple scattering approach, starting from a muffin tin approximation of the molecular potential. The Fe−heme structure has been obtained by analyzing independently the Extended X-ray Absorption Fine Structure (EXAFS) region and the X-ray Absorption Near Edge Structure (XANES) region. The EXAFS structural results are in full agreement with the crystallographic values of the models, with an accuracy of ± 0.02 Å for Fe-ligand distances, and ±6° for angular parameters. All the XANES features above the theoretical zero energy (in the lower rising edge) are well accounted for by single-channel calculations, for both Fe(II) and Fe(III) hemes, and the Fe−N$_p$ distance is determined with the same accuracy as EXAFS. XANES evaluations of Fe-5th and Fe-6th ligand distances are determined with 0.04−0.07 Å accuracy; a small discrepancy with EXAFS (0.01 to 0.05 Å beyond the statistical error), is found for protein compounds. Concerns from statistical correlation among parameters and multiple minima in the parameter space are discussed. As expected, the XANES accuracy is slightly lower than what was found for polarized XANES on Fe(III)MbCN single crystal (0.03−0.04 Å), and states the actual state-of-the-art of XANES analysis when used to extract heme-normal parameters in a solution spectrum dominated by heme-plane scattering.

Introduction

The accurate knowledge, at atomic resolution, of the Fe−heme structure in hemeproteins is increasingly required in studies of structural biology as far as it is now clear that subtle bond distance changes can be often sufficient for the Fe−heme active site to perform, or to trigger, its biological function. Heme-based sensors are typical examples where the heme center is directly concerned with regulation,[1−3] while in many other cases it may function in reversible binding of ligands or electron transfer.[4,5] Cytochrome P450s represent a third large class of heme-containing enzymes that

* To whom correspondence should be addressed. E-mail: p.dangelo@caspur.it (P.D.), dlonga@caspur.it (S.D.L.).
† Dipartimento di Chimica, Università di Roma "La Sapienza".
‡ Istituto CNR di Metodologie Chimiche-IMC, Sezione Meccanismi di Reazione, Dipartimento di Chimica, Università di Roma "La Sapienza".
§ Laboratori Nazionali di Frascati, INFN CP13.
|| Università Cattolica del Sacro Cuore.
⊥ EMBL, Hamburg.
Università dell'Aquila.

(1) Spiro, T. G.; Jarzecki, A. A. *Curr. Opin. Chem. Biol.* **2001**, *5*, 715–723.
(2) Gilles-Gonzalez, M. A.; Ditta, G. S.; Helinski, D. R. *Nature* **1991**, *350*, 170–172.
(3) Gilles-Gonzalez, M. A.; Gonzalez, G. *J. Inorg. Biochemistry* **2005**, *99*, 1–22.

10.1021/ic800982a CCC: $40.75
Published on Web 10/07/2008

catalyze the metabolism of multitudes of both endogenous and exogenous substrates where the active site is always the prosthetic group.[6,7]

Only in very few examples is the X-ray diffraction (XRD) structure of a protein single crystal known with sufficient resolution to explain the functional diversity of the heme site as well as the presence of conformers involved in the dynamics of Fe−heme in the same protein.[8] Quantum-mechanical atomistic simulation is a tool to enhance resolution,[1,9,10] however, the availability of a local, highly structure-sensitive experimental technique providing information on the Fe−heme structure at atomic or subatomic resolution is highly desirable.

X-ray Absorption Spectroscopy (XAS) is an important tool to probe the atomic environment of metals both in solid and solution state, though XAS applications to the study of condensed matter lacking long-range order (solutions or biological systems) has been less frequent. As an example, XAS was crucial to determine the basicity of the oxoiron(IV) in chloroperoxidase compound II, a finding that has strong implications in the understanding the cytochrome P450 oxygenation cycle.[11] A theoretical approach which uses pair distribution functions to model the extended X-ray absorption fine structure (EXAFS) signal has been developed and successfully applied to the quantitative structural investigation of liquid systems.[12,13] Conversely, owing to the lack of suitable theoretical tools, the modeling of the X-ray absorption near-edge structure (XANES) spectra of disordered systems has been quite crude or sometime completely impossible. In the past years an improved method (MXAN) of extracting the metrical and angular structural information available in XANES spectra has been developed.[14] The first application of this procedure has been the study of the structure of the Fe−heme in carbonmonoxy-myoglobin (low spin Fe(II)MbCO) and of its low temperature photolysis product (high spin Fe(II)Mb*CO) in single crystals.[15] It turned out evident that, as in EXAFS, the geometry of the molecule, rather than its electronic structure (i.e., iron valence state, spin state), is the main determinant of the XANES spectrum, and therefore, the correct structure can be recovered by MXAN with an accuracy of ±0.02−0.07 Å. The MXAN simulation reproduced both the dramatic spectral changes following the rupture of the Fe−CO bond in the XANES spectrum polarized along the bond direction and the weak variations of the spectrum polarized along the heme plane, following the restrained heme relaxation.[16] This method was then successfully applied to the analysis of several model systems and metalloproteins,[17−28] both in the solid state and in solution, allowing a quantitative extraction of the relevant geometrical information about the absorbing site.

In an X-ray absorption spectrum, the XANES region of the full multiple-scattering (MS) regime and the EXAFS region of the intermediate and single (SS) scattering regime are computationally analyzed in different ways, that is, by solving the exact scattering matrix inversion problem by XANES and by series expansion of the inverse matrix with selection of the main terms by EXAFS. The exact matrix inversion becomes a too heavily computational task at higher energies; conversely, the series expansion becomes infinite at lower energy, and therefore, it is still unpractical to develop a unique analysis tool accounting for the full XAS spectrum. Thus, joining EXAFS and XANES analysis seems the best way to extract the information contained in a full XAS spectrum and to establish the reliability of XANES analysis. Nowadays, the XANES theory is still in progress, and it would be very important to eliminate the need of a phenomenological treatment of some aspects, as performed in the MXAN procedure. Theoretical efforts[29] address the inclusion of vibrational effects in the high-energy part of the spectrum, the elimination of the muffin-tin (MT) approximation, the implementation of a multichannel multiple scattering theory, and the solution of the problem of the optical potential in the

(4) Antonini, E.; Brunori, M. *Hemoglobin and Myoglobin in their Reactions with Ligands*; North-Holland: Amsterdam, The Netherlands, 1971.
(5) Moore, G. R.; Pettygrew, G. W. *Cytochrome c: evolutionary structural and physiochemical aspects*; Springer-Verlag: Berlin, 1990.
(6) Makino, M.; Sugimoto, H.; Shiro, Y.; Asamizu, S.; Onaka, H.; Nagano, S. *Proc. Natl. Acad. Sci. U.S.A.* **2007**, *104*, 11591–11596.
(7) Schlichting, I.; Berendzen, J.; Chu, K.; Stock, A. M.; Maves, S. A.; Benson, D. E.; Sweet, R. M.; Ringe, D.; Petsko, G. A.; Sligar, S. G. *Science* **2000**, *287*, 1615–1622.
(8) Kondrashov, D. A.; Roberts, S. A.; Weichsel, A.; Montfort, W. R. *Biochemistry* **2004**, *43*, 13637–13647.
(9) Ryde, U.; Nilsson, K. *J. Am. Chem. Soc.* **2003**, *125*, 14232–14233.
(10) Bikiel, D. E.; Boechi, L.; Capece, L.; Crespo, A.; De Biase, P. M.; Di Lella, S.; Gonzales Lebrero, M. C.; Marti, M. A.; Nadra, A. D.; Perissinotti, L. L.; Scherlis, D. A.; Estrin, D. A. *Phys. Chem. Chem. Phys.* **2006**, *8*, 5611–5628.
(11) Green, M. T.; Dawson, J. H.; Gray, H. B. *Science* **2004**, *304*, 1653–1656.
(12) D'Angelo, P.; Di Nola, A.; Filipponi, A.; Pavel, N. V.; Roccatano, D. *J. Chem. Phys.* **1994**, *100*, 985–994.
(13) D'Angelo, P.; Barone, V.; Chillemi, G.; Sanna, N.; Meyer-Klaucke, W.; Pavel, N. V. *J. Am. Chem. Soc.* **2002**, *124*, 1958–1967.
(14) Benfatto, M.; Della Longa, S. *J. Synchrotron Radiat.* **2001**, *8*, 1087–1094.
(15) Della Longa, S.; Arcovito, A.; Girasole, M.; Hazemann, J. L.; Benfatto, M. *Phys. Rev. Lett.* **2001**, *87*, 155501–155504.
(16) Vojtechovsky, J.; Chu, K.; Berendzen, J.; Sweet, R. M.; Schlichting, I. *Biophys. J.* **1999**, *77*, 2153–2174.
(17) Arcovito, A.; Lamb, D. C.; Nienhaus, G. U.; Hazemann, J. L.; Benfatto, M.; Della Longa, S. *Biophys. J.* **2005**, *88*, 2954–2964.
(18) Benfatto, M.; Della Longa, S.; Natoli, C. R. *J. Synchrotron Radiat.* **2003**, *10*, 51–57.
(19) Benfatto, M.; D'Angelo, P.; Della Longa, S.; Pavel, N. V. *Phys. Rev. B.* **2002**, *65*, 174201–174205.
(20) D'Angelo, P.; Benfatto, M.; Della Longa, S.; Pavel, N. V. *Phys. Rev. B* **2002**, *66*, 0642091–0642097.
(21) D'Angelo, P.; Lucarelli, D.; Della Longa, S.; Benfatto, M.; Hazemann, J. L.; Feis, A.; Smulevich, G.; Ilari, A.; Bonamore, A.; Boffi, A. *Biophys. J.* **2004**, *86*, 3882–3892.
(22) Hayakawa, K.; Hatada, K.; D'Angelo, P.; Della Longa, S.; Natoli, C. R.; Benfatto, M. *J. Am. Chem. Soc.* **2004**, *126*, 15618–15623.
(23) Frank, P.; Benfatto, M.; Szilagyi, R. K.; D'Angelo, P.; Della Longa, S.; Hodgson, K. O. *Inorg. Chem.* **2005**, *44*, 1922–1933.
(24) Arcovito, A.; Moschetti, T.; D'Angelo, P.; Mancini, G.; Vallone, B.; Brunori, M.; Della Longa, S. *Arch. Biochem. Biophys.* **2008**, *475*, 7–13.
(25) Sepulcre, F.; Proietti, M. G.; Benfatto, M.; Della Longa, S.; Garcia, J.; Padros, E. *Biophys. J.* **2004**, *87*, 513–520.
(26) Della Longa, S.; Arcovito, A.; Benfatto, M.; Congiu-Castellano, A.; Girasole, M.; Hazemann, J. L.; Lo Bosco, A. *Biophys. J.* **2003**, *85*, 549–558.
(27) Della Longa, S.; Benfatto, M. *Recent Res. Dev. Proteins* **2002**, *1*, 317–343.
(28) Arcovito, A.; Benfatto, M.; Cianci, M.; Hasnain, S. S.; Nienhaus, K.; Nienhaus, G. U.; Savino, C.; Strange, R. W.; Vallone, B.; Della Longa, S. *Proc. Natl. Acad. Sci. U.S.A.* **2007**, *104*, 6211–6216.
(29) Natoli, C. R.; Benfatto, M.; Della Longa, S.; Hatada, K. *J. Synchrotron Radiat.* **2003**, *10*, 26–42.

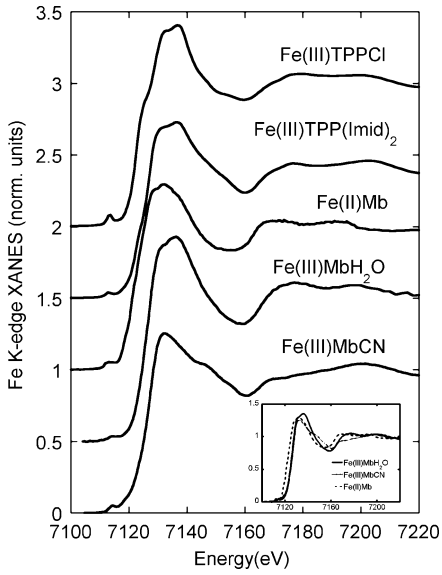

Figure 1. XANES spectra of hemes and hemeproteins. From top to bottom: Fe(III)TPPCl, Fe(III)TPP(Imid)$_2$, Fe(II) Mb, Fe(III) Fe(III)MbH$_2$O, and Fe(III)MbCN. Inset: overlay of the protein XANES spectra.

final state. A combined EXAFS and XANES data analysis was previously employed to investigate metal ions in solution,[19,20] hexacyanoferrat complexes,[22] and neuroglobin[23] (a myoglobin-like hemeprotein expressed in the brain of vertebrates). In the present paper we have systematically applied this combined approach to unveil the iron coordination environment in the porphynato complexes iron(III) tetraphenylporphyrin chloride (Fe(III)TPPCl) and iron(III) tetraphenylporphyrin bis(imidazole) (Fe(III)TPP(Imid)$_2$), and myoglobin in the iron(II) deoxy (Fe(II)Mb), iron(III) metaquo (Fe(III)MbH$_2$O), and iron(III) cyanomet form (Fe(III)MbCN). The XANES spectra of these compounds are shown in Figure 1. One important goal of this work is to assess the validity and accuracy of the MXAN method to the analysis of hemes and hemeproteins in solution. In particular, we are interested in the extraction of the axial heme parameters from the XAS spectra, and to this end we have selected Fe−heme compounds having different axial coordination and geometry. In spite of the fact that the XAS spectrum is dominated by the strong heme-plane scattering signal, Figure 1 clearly shows relevant differences among the spectra, and it is known that the XANES fingerprints of hemes and hemeproteins are diagnostic of their axial coordination.[27] In the inset of the figure, the overlay of the protein spectra allows one to better appreciate the differences and supports the uniqueness of each XANES fit shown in the XANES Results section. Note that, in spite of their large number, heme-plane pathways and their structural parameters are constrained (or highly restrained) because of the rigidity of the porphyrin ring so that their overall contribution can be considered a rather constant "background signal" which is perturbed, in different ways, by different axial ligands.

In the present work, the sensitivity and the accuracy of the MXAN method in the extraction of the Fe−heme structure in hemeproteins is tested and compared with EXAFS and with XRD data known in the literature. Our results show that the combined use of EXAFS and XANES makes possible the acquisition of geometrical information not accessible by a single technique.

2. Materials and Methods

2.1. Experimental Data. Fe K-edge X-ray absorption spectra of Fe(III)TPPCl and Fe(III)TPP(Imid)$_2$ were recorded in transmission mode at ESRF on the bending magnet beamline BM29.[30] The storage ring was operating in 16-bunch mode with a typical current of 80 mA after refill. The spectra were collected by using a Si(311) double-crystal monochromator with the second crystal detuned by 50% for harmonic rejection. Fe(III)TPPCl was purchased from Aldrich and used as supplied. Fe(III)TPP(Imid)$_2$ was prepared as previously described.[31] The measurements were carried out at room temperature, the compounds were milled, and pellets of the appropriate amount of the porphynato complexes and boron nitride were used to collect the X-ray absorption spectra. Three spectra were recorded and averaged for each sample.

Horse heart myoglobin was purchased from Sigma and used without further purification. The lyophilized protein was dissolved in 1:3 glycerol-water solutions buffered with potassium phosphate buffer 50 mM pH 7 at a final concentration of 7 mM. Protein in solution was in the met form (Fe(III)MbH$_2$O), and both the cyanomet (Fe(III)MbCN) and deoxy (Fe(II)Mb) form were obtained starting from this same derivative. Fe(III)MbCN was obtained by adding NaCN to a final concentration of 30 mM, and Fe(II)Mb was obtained by adding an excess of sodium dithionite. The XAS spectra on the protein compounds were collected at 20 K in fluorescence mode at EMBL Hamburg EXAFS beamline by using an energy-resolving thirteen-element Ge detector of very high purity. Measurements were performed with a Si(111) double-crystal monochromator, and 50% harmonic rejection was achieved by slightly detuning the two crystals from parallel alignment.[32] The DORIS III storage ring was running at an energy of 4.4 GeV with positron currents between 70 and 40 mA. For each sample 10 spectra were recorded with a 7 s/point collection statistic and averaged after performing an absolute energy calibration.[33,34]

2.2. Data Analysis. XAS calculations are carried out starting from Fermi's golden rule to obtain the photoabsorption cross section within the dipole approximation. One important step is to calculate the final state of the photoelectron transition moment, which describes the physical process of scattering the electron photoemitted by the central atom by outer atoms. This is done in the framework of MS theory[29] using a MT approximation for the shape of the potential of the cluster of atoms included.

2.2.1. EXAFS Data Analysis. Metallo-porphyrins present a significant challenge for multiple-scattering analysis as a wide variety of scattering signals are expected to contribute to the EXAFS spectra because of the symmetry and rigidity of the porphyrin macrocycle. We have undertaken EXAFS analysis of the Fe(III)-TTPCl and Fe(III)TPP(Imid)$_2$ complexes in an effort to develop a data analysis strategy to be applied to other metallo-porphyrins of biological relevance.

The EXAFS data analysis has been performed using the GNXAS method, which is based on the theoretical calculation of the X-ray absorption fine structure signal and a subsequent refinement of the

(30) Filipponi, A.; Borowski, M.; Bowron, D. T.; Ansell, S.; De Panfilis, S.; Di Cicco, A.; Itiè, J.-P. *Rev. Sci. Instrum.* **2000**, *71*, 2422–2432.
(31) Collins, D. M.; Countryman, R.; Hoard, J. L. *J. Am. Chem. Soc.* **1972**, *94*, 2066–2072.
(32) Hermes, C.; Gilberg, E.; Koch, M. H. *Nucl. Instrum. Methods Phys. Res.* **1983**, *222*, 207–214.
(33) Pettifer, R. F.; Hermes, C. *J. Phys. Colloq.* **1986**, *C8*, 127–133.
(34) Pettifer, R. F.; Hermes, C. *J. Appl. Crystallogr.* **1985**, *18*, 404–412.

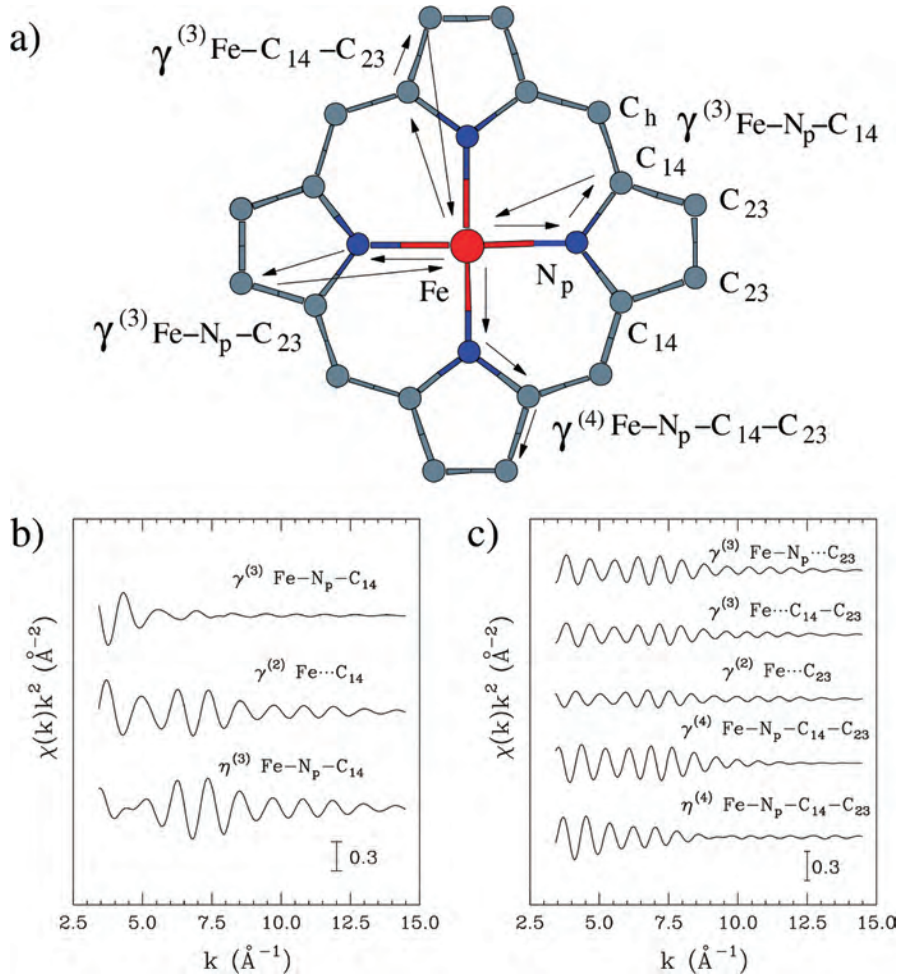

Figure 2. EXAFS MS signal contributions according to the GNXAS analysis program. (a) Sketch of the porphyrin macrocycle. Three-body $\gamma^{(3)}$ and four-body $\gamma^{(4)}$ pathways are indicated by arrows. (b) Relative Fe K-edge EXAFS strengths of the two contributing pathways in the Fe−N_p−C_{14} three-body configuration. (c) Relative Fe K-edge EXAFS strengths of the four contributing pathways in the Fe−N_p−C_{14}−C_{23} four-body configuration.

structural parameters. The theoretical framework of the GNXAS method is described in detail in previous publications.[35,36] In the GNXAS approach, the interpretation of the experimental data is based on the decomposition of the $\chi(k)$ signal into a summation over n-body distribution functions $\gamma^{(n)}$ calculated by means of the MS theory. Starting from the crystallographic structure of the Fe(III)TTPCl complex, we have calculated all possible scattering paths associated with the porphyrin ring. Obviously, the two-body single-scattering terms have to be considered at first. In Figure 2a, a sketch of the porphyrin macrocycle is shown together with all of the three- and four-body contributions which have to be included in the analysis. Note that despite the complexity of the system, only a relative small number of MS signals have been found to provide substantial contribution (Figure 2b, 2c). These paths include the three-body and four-body distributions of atoms belonging to the pyrrol rings, while the MS signals associated with atomic configurations including the C_h atoms of the porphyrin macrocycle have rather small amplitudes. Previous investigations on model compounds have confirmed that a quantitative EXAFS analysis of metallo-porphyrins requires a proper treatment of MS four-body terms.[37] The inclusion of these higher order contributions is essential to obtain a good agreement between theoretical and experimental data.

The structural parameters used in the minimization procedure are the bond distance (R) and bond variance (σ^2_R) for a two-body signal, the two shorter bond distances, the intervening angle (θ), and the six covariance matrix elements for a three-body signal. The four-body configurations are described by six geometrical parameters, namely the three bond distances, two intervening angles (θ and ϕ), and the dihedral angle (Ψ) defining the spatial orientation of the three bonds.

One advantage of the GNXAS method, as compared to other EXAFS data analysis procedures, is that the SS and MS signals depend on the same structural parameters that are the actual bond lengths and angles of the molecule under investigation. For example the three-body distribution Fe−N_p−C_{14} gives rise to a two-body signal, the $\gamma^{(2)}$ Fe···C_{14}, and to a MS signal, the $\gamma^{(3)}$ Fe−N_p−C_{14}. These two contributions have a similar frequency and depend on the same structural parameters namely the Fe−N_p distance, the N_p−C_{14} distance, and the Fe−N_p−C_{14} angle. For this reason they are usually added in a total contribution which is indicated as $\eta^{(3)}$ Fe−N_p−C_{14}. The relative amplitude and the frequency of these contributions are shown in Figure 2b for the Fe(III)TPPCl complex. Note that the signals have been calculated with a multiplicity of four and disorder effects have been introduced using a Debye−Waller factor. Similarly, a typical four-body distribution Fe−N_p−C_{14}−C_{23}

(35) Filipponi, A.; Di Cicco, A.; Natoli, C. R. *Phys. Rev. B* **1995**, *52*, 15122–15134.
(36) Filipponi, A.; Di Cicco, A. *Phys. Rev. B* **1995**, *52*, 15135–15149.
(37) Zhang, H. H.; Filipponi, A.; Di Cicco, A.; Scott, M. J.; Holm, R. H.; Hedman, B.; Hodgson, K. O. *J. Am. Chem. Soc.* **1997**, *119*, 2470–2476.

Table 1. XANES Analysis: Values of Parameters Used for Potential Calculation and Phenomenological Broadening

	Fe(III)TPPCl (high-spin)	Fe(III)TPP(Imid)$_2$ (low-spin)	Fe(II)Mb (high-spin)	Fe(III)MbH$_2$O (high-spin)	Fe(III)MbCN (low-spin)
no. of struct params	3	2	4	5	6
total no. of params[a]	9	8	10	11	12
			Phenomenological Broadening		
E_s^{normal} (±4 eV)[b]	20.6	7.9	21.5	20.02	11.7
A_s^{normal} (±4 eV)	11.1	15.3	6.9	7.0	13.4
E_s^{heme} (±4 eV)[b]	16.8	6.8	13.8	12.8	4.8
A_s^{heme} (±4 eV)	8.1	7.5	7.8	5.8	13.7
			Potential		
V_{0imp} (±2 eV) [b]	−7.72	−4.24	−7.26	−8.27	−7.59
ovlp (±2%)	−2.6	4.0	−6.5	4.0	6.9

[a] Optimization of the six nonstructural parameters, and evaluation of their respective statistical errors, have been obtained by preliminary tests of the MXAN procedure carried out by leaving these parameters free while keeping the structure fixed. [b] Values of E_s^{normal}, E_s^{heme}, and V_{0imp} are given in the theoretical energy scale where the zero corresponds to the continuum level.

includes the $\gamma^{(2)}$ Fe···C_{23}, two three-body MS terms $\gamma^{(3)}$ Fe−N_p···C_{23} and $\gamma^{(3)}$ Fe···C_{14}−C_{23}, and one four-body MS term $\gamma^{(4)}$ Fe−N_p−C_{14}−C_{23}. Also in this case, as these four contributions have a similar frequency (see Figure 2c) and depend on the same structural parameters, they are added in a total contribution named $\eta^{(4)}$ Fe−N_p−C_{14}−C_{23}. Figure 2c shows the relative strengths of the four contributing signals in the Fe−N_p−C_{14}−C_{23} four-body configuration; the four components have similar amplitudes, at variance with linear four-body signals which have a dominant $\gamma^{(4)}$ character. Note that when a four-body signal is included, the increase of fitting parameters is quite small as the four-body pathways contain some of the three-body pathways used in the fit; therefore, the same parameters describing these three-body pathways were used in the four-body case. Figures 2b and 2c put well in evidence what is known from theory: the contribution of the multiple scattering $\gamma^{(3)}$ and $\gamma^{(4)}$ terms with respect to single scattering terms increases at low energy, below about 7 Å^{-1}, and becomes rather strong below 4−5 Å^{-1}, that is, in the XANES regime. It is important to stress that the four-body MS treatment allows the extraction of additional structural information which is important in metallo-porphyrin chemistry. In particular, the quantitative determination of the structural parameters associated with the four-body distribution provides a direct estimation of the Fe displacement from the average porphyrin plane and the distortion of the tetrapyrrole macrocycle.

The EXAFS data analysis of all our samples has been performed generating a model spectrum starting from the crystallographic structures by adding all the relevant SS and MS contributions. Phase shifts were calculated using the standard MT approximation. The model $\chi(k)$ was then refined against the experimental data by using a least-squares minimization procedure in which structural and nonstructural parameters were allowed to float. Coordination numbers were fixed at the known crystallographic values. Two nonstructural parameters were minimized, namely E_0 (core ionization threshold) and S_0^2 (many body amplitude reduction factor). The quality of the fits was determined by the goodness-of-the-fit parameter $\mathscr{R}$[36] and by careful inspection of the EXAFS residuals and their Fourier Transforms (FT).

2.2.2. XANES Data Analysis. The MXAN fitting procedure has been applied to heme model systems and proteins on the space of structural and nonstructural parameters that are important in the potential definition and in mimicking electronic damping by a phenomenological function ($\Gamma(E)$, described below). In the final optimization loop of MXAN, all of these parameter are kept fixed. The nonstructural parameters obtained from this approach are reported in Table 1.

Atomic MT radii are calculated on the basis of the Norman criterion[38] including overlap between MT spheres that is optimized by fitting the ovlp parameter (only one parameters for the entire set of MT radii). The choice of MT radii fixes the constant MT potential V_0 and the charge densities within each MT sphere. Different values of ovlp, within reasonable values (between −7% and 7%), change the goodness of the fit but without relevant effects in the structural parameters determination. We obtained negative ovlp for penta-coordinate hemes and positive ovlp for hexa-coordinate hemes. As in penta-coordinate hemes the first shell distance is longer than in hexacoordinate hemes (2.06−2.07 A vs 1.98−2.0), it means that the optimal MT radius for the iron is nearly constant.

V_{0imp} is the value of the muffin-tin potential (V_0) when it is refined to best fit heme model compounds. The potential generator of MXAN (program VGEN) calculates this parameter automatically, and ovlp is the only potential parameter usually fitted as it is the only free parameter of the multiple scattering theory with the muffin-tin approximation. However according to this set of calculations, refining V_{0imp} provides an improvement both in χ^2 and in the accuracy of structural results, especially concerning axial parameters. An averaged value of −6.5 ± 2.0 eV can be considered a good calibration value for the systems under study. The porphyrin macrocycle, and the ligand molecules, were included in XANES analysis. The cluster size and the l_{max} value (i.e., the maximum l-value of the spherical harmonic expansion of the scattering path operators) were chosen on the basis of a convergence criterion. The experimental resolution is taken into account by a Gaussian convolution (0.6−0.8 eV). The real part of the exchange term was calculated using the Hedin−Lundqvist energy-dependent potential,[39] while all of the inelastic losses were taken into account by a phenomenological method previously described in detail.[18] According to this method, inelastic processes are accounted for by a convolution with a broadening function, with a width Γ given by $\Gamma = \Gamma_c + \Gamma(E)$. The constant part Γ_c includes contributions from the core-hole lifetime (1.2 eV, Lorentzian convolution) while the energy dependent term $\Gamma(E)$ (Lorentzian convolution) represents the inelastic processes.

$\Gamma(E)$ is zero below an onset energy E_s and begins to increase from a value A_s following the universal functional form related to the mean free path in a solid.[40] This method introduces three nonstructural parameters that are derived during the fit on the basis of a Monte Carlo search at each step of computation. One expects the accuracy of the structural parameters extracted from solution samples to be worse than those determined for the Fe(II)MbCO single crystal previously studied[15] because of the convolution of

(38) Norman, J. G. *Mol. Phys.* **1974**, *81*, 1191–1198.
(39) Hedin, L.; Lundqvist, B. I. *J. Phys. C* **1971**, *4*, 2064–2083.
(40) Müller, J. E.; Jepsen, O.; Wilkins, J. W. *Solid State Commun.* **1982**, *42*, 365–369.

the polarized contributions in the solution spectrum. Another difficulty arises from the use of the phenomenological $\Gamma(E)$ function: because of the strong asymmetry of the Fe−heme site, the function used to fit unpolarized spectra of a system with approximately C_{4v} symmetry has a vectorial form with different values of the E_s and A_s parameters for the two polarized components of the spectrum. In total, five nonstructural parameters, Γ_c, E_s^{normal}, E_s^{heme}, A_s^{normal}, A_s^{heme} are used in the fitting procedure. Theoretically, this approach is justified considering that all of the physical quantities involved, in particular the dielectric function associated with the calculation of the self-energy of the system, must have the same symmetry of the geometrical cluster. As a consequence, the mean free path term is largely anisotropic, as it is evident by looking at the systematic difference in the values E_s found for the $\varepsilon \parallel$ c and $\varepsilon \parallel$ a* polarized spectra of the Fe(II)MbCO crystal.[15] The values used for each heme compound are listed Table 1. These parameters show a rather large degree of intercorrelation, however, values of E_s^{normal} and E_s^{heme} seem systematically lower in low-spin Fe−hemes with respect to high-spin Fe−hemes.

A constant experimental error of 0.012 normalized units (i.e., units for which the absorption jump is equal to 1) was chosen. The minimization of the χ^2 function was performed in the space of the n selected structural parameters.

The fit includes a minimal number of selected parameters: they are the core size, the Fe-displacement, the Fe-N_{his} and Fe-6th ligand distances for hexa-coordinated heme systems. In the case of cyanomet-myoglobin, also the bending angle between the Fe−C−N vector and the C−N bond and the C−N bond length were considered. During the fit, the outer atoms of the imidazole ring of the histidine and of the pyrrol rings of the porphyrin rigidly followed the motion of the N_{his} and N_p atoms, respectively.

3. EXAFS Results

3.1. EXAFS Analysis of Fe(III)TPPCl and Fe(III)TPP(Imid)$_2$. First, we have carried out a thorough EXAFS data analysis of two porphyrin models whose X-ray structure is known with an estimated error on structural parameters of about 0.004−0.005 Å.[31,41] The results are shown in Figure 3. In the Fe(III)TPPCl complex the iron atom is pentacoordinated and, according to the X-ray diffraction determination,[41] it lies 0.6 Å out of the heme plane. Conversely, in Fe(III)TPP(Imid)$_2$ the iron atom has two imidazole molecules in the axial positions and it lies on the heme plane.[42] The main structural differences between the two models are the presence of different ligands in the axial positions and the Fe−N_p distance which is about 0.08 Å longer in Fe(III)TPPCl than in Fe(III)TPP(Imid)$_2$. The two XAS spectra have been collected in transmission mode, resulting in a noise level of 8×10^{-5} and 1×10^{-4} for Fe(III)TPPCl and Fe(III)TPP(Imid)$_2$, respectively. The Fe(III)TPPCl EXAFS spectrum is dominated by the first-shell two-body signals associated with the four nitrogen atoms from the porphyrin ($\gamma^{(2)}$ Fe−N_p) and the axial chloride atom ($\gamma^{(2)}$ Fe−Cl). In addition to the first-shell contributions, the simulation requires four carbon atoms at about 3.4 Å derived from the connecting methylene groups ($\gamma^{(2)}$ Fe···C_h). A detailed analysis of the MS terms of this system has been carried out starting from the crystallographic structure, and it has been found that the main contribution to the absorption coefficient arises from the MS signals of third and fourth order associated with the Fe−N_p−C_{14}−C_{23} four-body configurations. It should be pointed out that even if this pathway is not linear, the amplitude of the MS signals is strongly enhanced by the porphyrin-induced multiplicity of eight. A good fit of the experimental data required the inclusion of the Fe−N_p−C_{14} three-body ($\eta^{(3)}$) and the Fe−N_p−C_{14}−C_{23} four-body ($\eta^{(4)}$) total contributions. The former term is quite strong and becomes more intense at higher k while the amplitude of the four-body total signal $\eta^{(4)}$ becomes negligible for k values higher than 9 Å^{-1}. The analysis of the Fe(III)TPP(Imid)$_2$ spectrum is more complex as together with the SS and MS scattering signals of the porphyrin ring it is necessary to include the contributions associated with the two imidazole molecules. In particular, the EXAFS data analysis has been carried out treating the contributions associated with the axial ligands as separate signals as the Debye−Waller factors associated with the porphyrin plane could be different from those of the axial ligands because of the rigidity of the ring, on one hand, and to the different coordination distances (1.96 and 1.99 Å) of the two histidines, as determined by XRD, on the other. However, because of the lattice constraints of this small molecule crystal, from EXAFS data analysis we obtained similar axial and planar Debye−Waller and distance values (see Tables 2 and 3). The EXAFS spectrum is dominated by the first-shell two-body signals associated with the four nitrogen atoms from the porphyrin and the two axial nitrogen atoms from the imidazole molecules. The amplitude of the three-body and four-body signals arising from the imidazole molecules are much lower than the corresponding contributions of the plane, both due to the higher multiplicity and to the rigidity of the porphyrin ring. It is important to stress that, notwithstanding the strong contributions to the spectra associated with the tetrapyrrole macrocycle, the experimental EXAFS data of the two model complexes are quite different all over the k range, showing the sensitivity of EXAFS to the fine structural details, and to the nature and geometry of the axial ligands. The agreement between the fitted theoretical $\chi(k)$ signals and the experimental data shown in Figure 3 is very good, proving the reliability of the MS scheme used in the analysis.

The FT moduli of the Fe(III)TPPCl and Fe(III)TPP(Imid)$_2$ experimental spectra extracted with a three segmented cubic spline are shown in the lower panels of Figure 3. The FTs have been calculated in the interval k = 2.8−14.5 Å^{-1} with no phase-shift correction applied. The first peak of the FT spectra is associated with the

(41) Scheidt, W. R.; Finnegan, M. G. *Acta Crystallogr., Sect. C* **1989**, *45*, 1214–1216.
(42) Vojtechovsky, J.; Chu, K.; Berendzen, J.; Sweet, R. M.; Schlichting, I. *Biophys. J.* **1999**, *7*, 2153–2174.
(43) Powers, L.; Sessler, J. L.; Woolery, G. L.; Chance, B. *Biochemistry* **1984**, *23*, 5519–5523.
(44) Scherk, C. G.; Ostermann, A.; Achterhold, K.; Iakovleva, O.; Nazzikol, C.; Krebs, B.; Knapp, E. W.; Meyer-Klaucke, W.; Parak, F. G. *Eur. Biophys. J.* **2001**, *30*, 393–403.
(45) Cruickshank, D. W. *Acta Crystallogr., Sect. D* **1999**, *55*, 583–601.
(46) Bolognesi, M.; Rosano, C.; Losso, R.; Borassi, A.; Rizzi, M.; Wittenberg, J. B.; Boffi, A.; Ascenzi, P. *Biophys. J.* **1999**, *77*, 1093–1099.

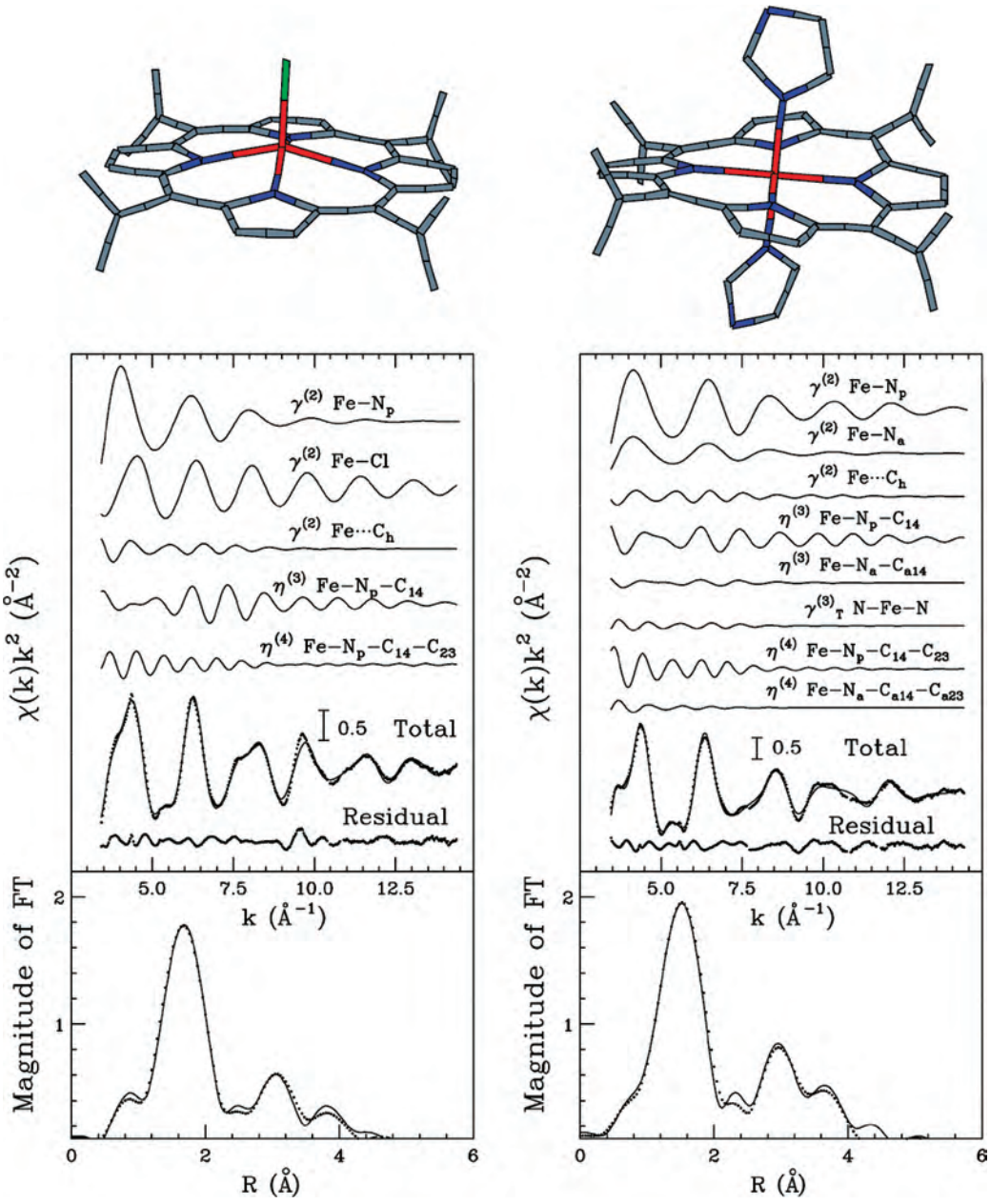

Figure 3. Fe K-edge analysis of porphynato complexes via the GNXAS program: Left panel, Fe(III)TPPCl: from top to bottom two-body SS, three-body MS, and four-body MS signals included in the fit, total signal superimposed to the experimental one, residual curve, and fit in the Fourier Transformed (FT) space. Right panel, the same analysis is done for Fe(III)TPP(Imid)$_2$. Because of the presence of imidazole rings as axial ligands, two extra MS signal have to be included: $\eta^{(3)}$ Fe−N$_a$−C$_{a14}$ and: $\eta^{(4)}$ Fe−N$_a$−C$_{a14}$−C$_{a23}$. The difference between peripheral nitrogens and carbons of the imidazole ring is neglected.

first coordination shell around the iron. It comprises four pyrrolic nitrogen atoms of the porphyrin ring and one chloride atom in the case of Fe(III)TPPCl and six nitrogen atoms in the case of Fe(III)TPP(Imid)$_2$. The second and third peaks contain all of the SS and MS contributions associated with the atoms in the second and third coordination shells of the porphyrin plane in the former complex, while an additional contribution associated with the axial imidazole molecules is present in the latter complex. Simple inspection of the FT spectra once more shows the sensitivity of the EXAFS technique toward structural changes in metallo-porphyrins. The first important observation is that both the position and intensity of the FT first peaks are different as a consequence of the Fe−N$_p$ elongation and presence of different axial ligands. Moreover, the presence of the imidazole molecules in the axial positions gives rise to additional MS contributions to the spectrum, and this is reflected in the higher intensity of the second and third FT peaks for the Fe(III)TPP(Imid)$_2$ complex.

The structural parameters extracted from the EXAFS fitting procedure are compiled in Table 2, together with X-ray diffraction values reported in the literature,[41] and XANES analysis (see below). The Debye−Waller factors for each distance are listed in Table 3. The EXAFS analysis is in perfect agreement with the crystallographic determinations

Table 2. Comparison of the Structural Results Obtained from XANES, EXAFS, and XRD

	experiment	⟨Fe−Np⟩ (Å)	Fe−His (Å)	Fe−L1 (Å)	Bending	L1−L2	Fe−heme displ. (Å)[b]
Fe(III)TPPCl							
	XRD[41]	2.07(1)		2.211(1)			−0.57
	MS EXAFS[a]	2.08(1)		2.20(2)			−0.46(7)
	XANES[a]	2.04(2)		2.16(6)			−0.29(15)
Fe(III)TPP(Imid)$_2$							
	XRD[31]	1.99(1)	1.957(4)−1.991(4)				0.009
	MS EXAFS[a]	1.99(1)	1.99(2)				0.00(3)
	XANES[a]	1.99(3)	1.90(4)				
Fe(II)Mb							
	1.15 Å XRD[42]	2.07(3)	2.14(2)	3.52			0.39(1)
	SS EXAFS[43]	2.06	2.12				
	MS EXAFS[a]	2.06(1)	2.11(2)				
	XANES[a]	2.06(3)	2.15(5)	3.7(2)			0.2(2)
Fe(III)MbH$_2$O							
	1.1 Å XRD[42]	2.03(2)	2.14(1)	2.13(1)			0.138(4)
	SS EXAFS[43]	2.04	2.11	1.88			
	MS EXAFS[44]	2.02	2.10	2.11			
	MS EXAFS[a]	2.03(1)	2.14(2)	2.18(2)			
	XANES[a]	2.01(2)	2.14(6)	2.22(6)			
Fe(III)MbCN							
sperm whale	1.8 Å XRD[46]	2.03	2.02	2.02	166	1.06	
sperm whale	1.4 Å XRD[28]	2.04	2.08	1.92	167	1.11	
sperm whale	XANES crystal[28]	2.01(1)	2.07(3)	1.87(4)	170(7)	1.10(2)	
horse	EXAFS[a]	1.98(1)	2.07(2)	1.84(2)	171(6)	1.14(1)	
horse	XANES solution[a]	1.98(2)	2.01(7)	1.96(5)	166(20)	1.14(2)	

[a] This work. [b] Negative values, proximal displacement; positive values, distal displacement.

Table 3. EXAFS Analysis: Debye−Waller Factors (Å^2 or deg^2)

	Fe(III) TPPCl	Fe(III)TPP (Imid)$_2$	Fe(II) Mb	Fe(III) MbH$_2$O	Fe(III) MbCN
Fe−N$_p$	0.008	0.004	0.005	0.004	0.002
Fe−ligand	0.004	0.004		0.002	0.002
Fe−His		0.004	0.006	0.005	0.002
bending					5
Ψ angle	4	10	18	22	24

both for the planar and axial distances and for the iron-heme displacement. To establish error limits on the structural parameters, we have applied a statistical analysis using two-dimensional contour plots to selected parameters from the fit results. This analysis examines correlations among fitting parameters and evaluates statistical errors in the determination of the Fe coordination structure, which will be very useful in cases where the crystallographic data are not available. The approach has been described in detail elsewhere,[36] but in essence parameters with highest correlation dominate in the error estimate. From this analysis a strong statistical correlation has been found between the N_p-C_{14} and $C_{14}-C_{23}$ bond lengths, suggesting that the determination of the two distances has large effect on each other. However, the other refined parameters were remarkably stable, varying less than 0.02 Å and 3°, for distances and angles, respectively, and giving excellent agreement with the crystallographic values.[41] It is important to outline that the Ψ values obtained from the EXAFS analysis correspond to a Fe displacement from the average porphyrin plane of 0.46 ± 0.07 Å in the case of Fe(III)TPPCl, while the Fe atom has been found to lie in the plane for Fe(III)TPP(Imid)$_2$ in agreement with the crystallographic determinations.[42] Note that, as previously mentioned, the $\gamma^{(4)}$ signal depends on six structural parameters, one of which (the $Fe-N_p$ distance) is easily extracted from the first shell $\gamma^{(2)}$ signal. The other two structural parameters, namely, the N_p-C_{14} distance and the $Fe-N_p-C_{14}$ angle, are determined from the $\gamma^{(3)}$ signal. Of the three remaining parameters, the $C_{14}-C_{23}$ distance and the $Np-C_{14}-C_{23}$ angle are restrained from the rigidity of the pyrrolic ring and, therefore, only the dihedral angle, which is connected with the Fe−heme displacement, has to be refined on the basis of the $\gamma^{(4)}$ signal. An accurate determination of the Ψ angle relies on the possibility of extracting both the $\gamma^{(3)}$ and the $\gamma^{(4)}$ signals from the experimental data. Even if the four-body signal vanishes for k values higher than 8 Å^{-1}, the beat pattern of the $\gamma^{(3)}$ $N_p-C_{14}-C_{23}$ signal extends to higher k values, and this makes it critical to have analyzable data in a wide k range.

3.2. EXAFS Analysis of Fe(II)Mb. In the second step of the investigation, the EXAFS data analysis has been applied to two hemeproteins whose X-ray structure is known at atomic resolution. In protein samples in solution the low concentration of the photoabsorber makes it necessary to collect the XAS data in fluorescence mode. The signal-to-noise ratio of these spectra is usually one order of magnitude worse than the model systems measured in transmission mode, reducing the k-interval and, consequently, the structural information contained in the EXAFS data. Fe(II)Mb does not present ligands in the sixth axial position allowing a reliable characterization of the SS and MS signals associated with the proximal histidine. The EXAFS data analysis of horse hearth Fe(II)Mb has been carried out starting from the crystallographic structure at atomic resolution (PDB code: 1A6N).[42] According to this structure, the Fe atom is coordinated with four pyrrolic nitrogen atoms at 2.07 ± 0.03 Å and one nitrogen atom of the axial histidine at 2.14 ± 0.02 Å. The Fe atom is out of the heme-plane with a displacement of 0.39 Å toward the proximal histidine. The results of the EXAFS data analysis, which has been performed using the same approach previously described, are shown in the left panels of Figure 4. The dominant contribution to the total $\chi(k)$ signal is due to the first shell

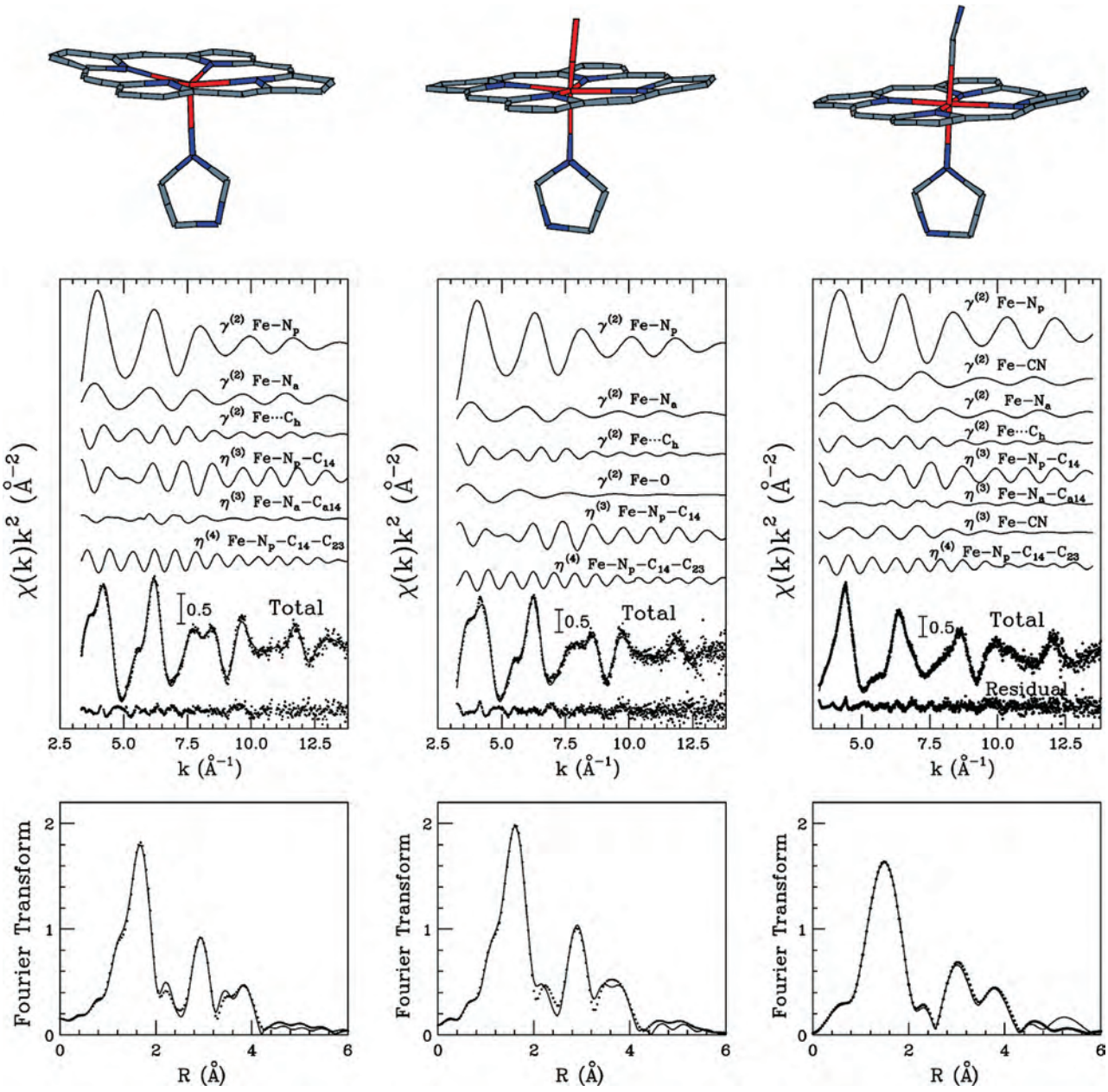

Figure 4. Fe K-edge EXAFS analysis of hemeproteins, in the same way as done for porphynato complexes of Figure 3: Fe(II)Mb (left), Fe(III)MbH$_2$O (center), and Fe(III)MbCN (right).

paths, namely the $\gamma^{(2)}$ Fe−N$_p$ with a 4-fold multiplicity, and the $\gamma^{(2)}$ Fe−N$_a$ relative to the axial imidazole nitrogen from the proximal histidine. Other contributions to the theoretical signal come from the $\gamma^{(2)}$ Fe···C$_h$, $\eta^{(3)}$ Fe−N$_p$−C$_{14}$, and $\eta^{(4)}$ Fe−N$_p$−C$_{14}$−C$_{23}$, while the three-body signal $\eta^{(3)}$ Fe−N$_a$−C$_{a14}$ associated with the axial histidine is non-negligible. Contrary to Fe(III)TPP(Imid)$_2$, the four-body contribution relative to the proximal histidine imidazole ring has a very weak amplitude, and it has been neglected in the analysis. The agreement between the theoretical and experimental spectra is excellent concerning both the $\chi(k)$ and the FT spectra and confirms the good accuracy of the EXAFS analysis when applied to hemeproteins. The structural parameters relative to the iron first shell distances derived from XRD,[42] an earlier SS EXAFS analysis reported in the literature,[43] and the present GNXAS analysis are compared in Table 2. Data are in excellent agreement. Moreover, other structural data are extracted from the GNXAS analysis, namely the Np−C$_{14}$ and C$_{14}$−C$_{23}$ average distances, 1.35 ± 0.02 Å and 1.39 ± 0.02 Å, respectively, in good agreement with the crystallographic values of 1.33−1.46 Å and 1.42−1.48 Å.[42] In this case the limited k-range (k = 2.8−13.7 Å^{-1}) used in the analysis hampers an accurate determination of the dihedral angle and, as a consequence, of the Fe−heme displacement. Also in this case the Debye−Waller factors associated with the bond distances are listed in Table 3.

3.3. EXAFS Analysis of Fe(III)MbH$_2$O. The second hemeprotein considered as a protein model system known at atomic resolution is horse heart metaquo-myoglobin (Fe(III)MbH$_2$O) at pH = 6.0. Water oxygen is the sixth axial ligand of the ferric high-spin heme in this derivative. Even

in this case, the EXAFS analysis has been carried out starting from the crystallographic structure solved at 1.1 Å resolution (PDB code: 1A6K)[42] in the range $k = 2.8-13.7$ Å^{-1}. According to this structure the Fe−Np distance is 2.03 ± 0.02 Å, the proximal histidine is coordinated at 2.14 ± 0.01 Å, and the water oxygen is coordinated at 2.13 ± 0.01 Å. The results of the EXAFS analysis are shown in Figure 4, central panel. Theoretical contributions to the $\chi(k)$ spectrum include the same signals as Fe(II)Mb, apart from the three-body signal $\eta^{(3)}$ Fe−N_a−C associated with the axial histidine which is neglected in this case because its amplitude is comparable with the noise level. In addition, the $\gamma^{(2)}$ Fe−O signal due to the presence of an axial water oxygen has to be included. In principle, the two axial distances, from a water oxygen and from a restrained imidazole ring, in the MS analysis, have to be treated separately and can be distinguished owing to the presence of MS contributions associated with the proximal histidine. On the other hand, as a result of the fit, the MS contributions of the proximal histidine turned out negligible, so in this specific case EXAFS cannot discriminate between the ligand type related to the 2.14 and 2.18 Å axial distances obtained from the minimization procedure (see Table 2). This is a case where an EXAFS ambiguity can be resolved by XANES (see below), so that the assignment of the axial distances in Table 2 has been made according to the XANES results. However, as previously determined from XRD, the Fe−N_a and Fe−O distances are equal within the reported statistical errors. The agreement between the experimental $\chi(k)$ and FT spectra and the calculated ones is excellent. The FT spectrum is calculated between 3.5 and 11.0 Å^{-1}. The structural parameters of the first coordination shell obtained from the minimization procedure are in good agreement (Table 2) with those reported by XRD[42] and previous SS[43] and MS[44] EXAFS studies apart from the sixth ligand distance. There is an evident discrepancy between the SS EXAFS analysis and the other structural determinations, which confirms the importance of including MS terms in the analysis. The axial distance determinations by MS EXAFS match the XRD value within 0.05 Å (i.e., with a 0.01−0.02 Å out of their respective statistical errors). Differences in the two MS EXAFS determinations could be due to the inclusion of the four-body contributions in the analysis. Also in this case the determination of the dihedral angle was hampered by the poor quality of the data at high energy, while the Debye−Waller factors are listed in Table 3.

3.4. EXAFS Analysis of Fe(III)MbCN. Last we have considered the cyanomet-myoglobin whose X-ray structure is known at lower resolution (1.4 Å, PDB code: 2JHO).[28] The bond lengths error on this structure has been estimated by using the Cruickshank Diffraction Precision Index DPI,[45] which at the reported resolution is about 0.05 Å for atoms with a B-factor of 18−20 Å^2. The EXAFS analysis has been carried out starting from the crystallographic structure using the same SS and MS signals of the porphyrin plane previously described for the model compounds, the $\eta^{(3)}$ Fe−N_a−C associated with the axial histidine, and the two-body $\gamma^{(2)}$ Fe−CN and the three-body $\gamma^{(3)}$ Fe−C−N associated with the CN axial ligand. These two latter signals, whose amplitude is very strong in the whole analyzed k-range, allowed us to determine the geometry of the axial ligand with high accuracy. The results obtained by the GNXAS minimization procedure performed in the k-range 2.8−13.7 Å^{-1}, are shown in Figure 4, right panel. The structural parameters are listed in Table 2, together with the XRD values corresponding to sperm whale myoglobin (PDB codes: 1EBC[46] and 2JHO[28] at 1.8 Å and at 1.4 Å resolution, respectively). The Fe−Np distance obtained from EXAFS is 1.98 ± 0.01 Å, the Fe−CN distance is 1.84 ± 0.02 Å, while the Fe−C−N angle is found to be equal to 171 ± 6°. Noticeably, these results are also in good agreement with polarized XANES obtained "in situ" from the same crystal (2JHO).[28] Debye−Waller factors are listed in Table 3.

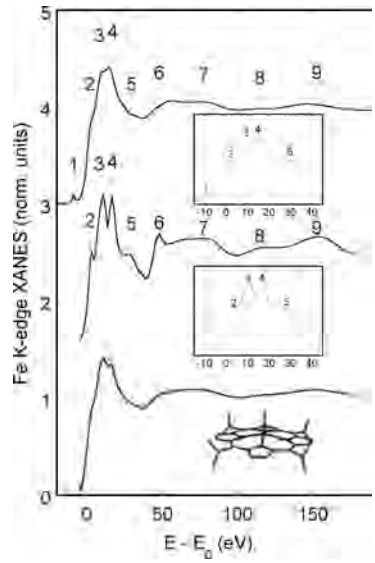

Figure 5. Fe K-edge XANES analysis of Fe(III)TPPCl, via the MXAN program. Top: experimental spectrum. Centre curve: XANES calculation without broadening terms. In the insets, the edge region is expanded. On the bottom, the experimental spectrum and best fitting theoretical spectrum, after broadening, are superimposed to check the fit quality.

4. XANES Results

In Figure 5, the XANES analysis of the first sample under investigation, Fe(III)TPPCl, is displayed. Up to nine features are present in the experimental spectrum (top curve) that are reproduced by MXAN at the end of the optimization procedure leading to the best fitting structure. The middle curve is the calculated XANES spectrum without any broadening factor. On the bottom of the figure, the theoretical spectrum after broadening (solid line) is superimposed to the experimental data (diamonds), showing the final quality of the fit. The insets in the same figure put in evidence the rising edge region. It is essential to include, beyond the first-shell ligands, the entire porphyrin ring (depicted in the figure) to reproduce all features from **2** to **9**; thus, in our approach these features represent final states of the photoelectron delocalized on the entire three-shell cluster. The calculated spectrum does not include the pre-edge feature **1**, as it is poorly reproduced by the MS analysis. It is well-known that, in the extended

continuum calculations, the amplitude of transition between the 1s orbital and bound states is not correctly reproduced because of an incorrect normalization of the final bound state wave function. In some cases, quadrupole effects may even play a role, which are completely neglected in the dipole approximation of the calculation. However, the main goal when using the MXAN method is not to accurately fit the pre-edge features but to recover the structure under study using an appropriate spectral range, starting from the rising edge, spanning the low energy region including the continuum XANES features, and extending up to the first part of the EXAFS region (up to 180 eV, corresponding to about 7 $Å^{-1}$). The low energy features **2**, **3**, and **4** are well reproduced by our calculations as single electron transitions to empty molecular states with p symmetry delocalized all over the molecular cluster. Peaks **3** and **4** are observed in calculated spectra as plane-polarized transitions. They arise after including the third shell of carbons of the porphyrin macrocycle. Thus, the origin of the fine structure of the main XANES feature seems different from what was proposed for the Fe(III) aqua-ion,[47,48] for which it was necessary to include a second electron transition channel to obtain a satisfactory reproduction of the XANES spectrum. The numerical values of structural parameters extracted by the MXAN optimization procedure for Fe(III)-TPPCl, and for all the other compounds under study, are compiled in Table 2. In the case of Fe(III)TPPCl, our EXAFS and XANES data coincide with reported measurements from XRD[41] within statistical errors. According to our analysis, the Fe−N_p distance, giving the main contribution to the XANES spectrum as well as to EXAFS, is measured with 0.02 Å accuracy, while a larger statistical error affects the Fe−Cl distance (0.06 Å). XANES probes the Fe−heme displacement with an accuracy of about 0.15 Å.

In Figure 6, MXAN best fits are shown for hexa-coordinate Fe(III)TPP(Imid)$_2$ and the two adducts of myoglobin known at atomic resolution, namely Fe(II)Mb and Fe(III)MbH_2O. In these three cases, the XANES best-fit parameters coincide with those obtained by XRD[31,42] and EXAFS, with two exceptions: in Fe(III)TPP(Imid)$_2$ the average distance of the axial Fe-imidazoles measured by XANES (1.90 ± 0.04Å) differs from those measured by XRD and EXAFS with a 0.03 Å discrepancy (out of the statistical errors); in Fe(III)MbH_2O the Fe-water distance (2.22A ± 0.06Å) is in agreement with MS EXAFS but it is 0.02 Å longer (out of statistical errors) than that measured by XRD. A possible explanation of these discrepancies for the heme axial distances is given in the discussion section.

In the case of pentacoordinate Fe(II)Mb, a noncoordinating oxygen 3.7 ± 0.2 Å far from the Fe center gives rise to a detectable contribution in the XANES, while it is not detected in EXAFS. This evidence perfectly agrees with the presence

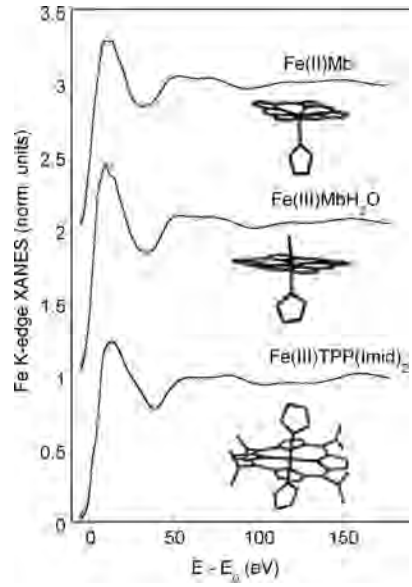

Figure 6. Fe K-edge XANES fit of Fe(III)TPP(Imid)$_2$, Fe(III)MbH_2O, and Fe(II)Mb.

of a protein docking site populated by water molecules in the hydrophobic distal pocket of deoxy-myoglobin.[42] Last, it is worth noting that contrary to EXAFS, since the XANES analysis is carried out in the photoelectron-wave interval 0−7 $Å^{-1}$ having a spectrum with lower S/N ratio, the Fe−heme displacement in Fe(II)Mb can be measured with the same accuracy as in the Fe(III)TPPCl model.

At last we have applied the MXAN procedure to Fe(III)-MbCN in solution. The structure of this protein has been reported at 1.4 Å resolution, with enhanced active site resolution,[28] as a result of a novel experiment combining X-ray diffraction and "in situ" XANES analyses, on the same crystal at the same beamline in the same experimental session. In Figure 7, top curve, the XANES spectrum of Fe(III)MbCN in solution is shown. It exhibits ten spectral features **1**−**10**. In the upper inset, a blow up of the same spectrum is displayed together with the XANES spectra for polarization along the heme_plane (dashed) and heme_normal (dotted), obtained from single crystal Fe(III)MbCN.[28] The spectrum in solution can be reproduced by a 2:1 linear combination of the heme-plane and heme-normal spectra, respectively, as expected for the approximate C_4 symmetry of the porphyrin. This similarity demonstrates that the structures of the Fe−heme−CN cluster in Fe(III)MbCN in solution (horse) and in the crystal (sperm whale) are identical within the experimental errors and allows us to compare directly four independent analysis methods on the same structure: (1) XRD in crystal, (2) polarized XANES in crystal, (3) unpolarized XANES in solution, and (4) EXAFS in solution. The comparison is reported in Table 2. We observe that the Fe−N_p and Fe−CN distances are slightly overestimated in XRD at 1.4 Å resolution, as compared to polarized XANES in the crystal, and EXAFS in solution. Overestimation becomes bigger for the Fe−CN distance, when considering the previously reported X-ray structure, PDB code = 1EBC at 1.8 Å resolution.[46] By comparing XANES and EXAFS in solution, there is another discrepancy

(47) Benfatto, M.; Solera, J. A.; Proietti, M. G.; Chaboy, J.; García, J. *Phys. Rev B* **1997**, *56*, 2447–2452.
(48) Benfatto, M.; Solera, J. A.; García, J.; Chaboy, J. *Chem. Phys.* **2002**, *282*, 441–450.

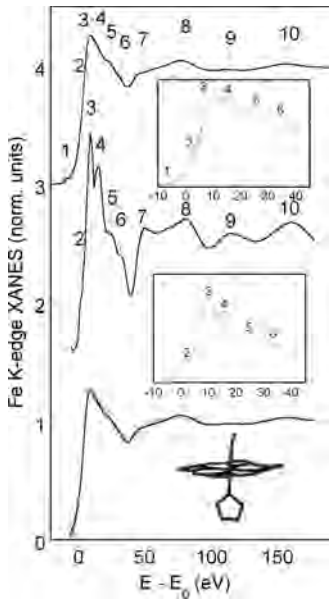

Figure 7. Fe K-edge XANES analysis of Fe(III)MbCN. Top: Experimental spectrum in solution. In the inset, the edge region is expanded and compared with the ε||heme_plane (dashed) and ε||heme_normal (dotted) polarized spectra of Fe(III)MbCN single crystal (Arcovito et al. 2007). Center: XANES calculation without broadening terms. In the inset, the edge region is expanded. Bottom: the experimental spectrum in solution and the best fitting theoretical spectrum, after broadening, are superimposed.

on the Fe−CN distance: (1.96 ± 0.05) Å and (1.84 ± 0.02) Å, respectively, 0.05 Å out of the statistical error. Note that the value measured for the same parameter by polarized XANES on single crystal, (1.87 ± 0.04) Å, is intermediate between them and in agreement within their statistical error. The C−N distance (1.14 ± 0.02) is identical to the EXAFS value and consistent with the value found for hexacyanoferrat(III) complexes by XRD, EXAFS, and XANES,[22] whereas the XRD determinations at 1.8 Å and 1.4 Å resolutions seem slightly underestimated. It is important to note that the determination of the Fe−C−N bending angle by XANES in solution (166 ± 20)° is in agreement with the others, in spite of its rather large error (five times larger than that found by polarized XANES on the crystal).[28] In the next section, the XANES sensitivity to the axial parameters in solution will be discussed.

5. Discussion

In the present work, we have systematically applied a fitting procedure to interpret both the XANES and EXAFS spectra of porphynato complexes and hemeproteins, using the whole energy range of the absorption spectrum for a quantitative determination of the structural parameters. As stated above, a discrepancy of 0.05 Å (or less) eventually exists between the XANES determinations and the values known by X-ray diffraction and EXAFS for the Fe-5th ligand and Fe-6th ligand distances. These discrepancies are representative of the actual accuracy of XANES studies when used to extract parameters of axial ligands in solution, where the signal is dominated by heme-plane scattering. This error is slightly higher than what was found (0.02−0.03 Å) by polarized XANES studies on crystalline Fe(III)MbCN[28] and Fe(II)MbCO.[15] In Fe(III)MbCN the Fe−CN distance measured by XANES in solution (1.96 ± 0.05 Å) is in agreement within the statistical errors with the 1.4 A resolution XRD and polarized XANES on the crystal and 0.05 Å out of the statistical error with respect to EXAFS. Of course, because of the convolution of the polarized contributions in the solution spectrum, one expects the accuracy of the axial parameters to be worse than in the reported angle resolved experiments where the strong heme scattering contribution can be depressed by the polarization dependence. However, these discrepancies indicate the presence of systematic errors. As observed during the simulation of polarized spectra of single crystal Fe(II)MbCO and Fe(II)Mb*CO,[15] for a chosen experimental error of 0.01 normalized units, the accuracy of the fit is better for the (ε || heme_normal) polarization, than for the (ε || heme_plane) polarization, by a factor of 1.5−2.0. We believe that systematic errors in the XANES analysis can arise mostly because of the poor approximation used for the phenomenological broadening function $\Gamma(E)$ that mimics the electronic damping. In all cases studied until now[15,19,20,22,26] such systematic errors did not appreciably affect the structural results, confirming how this spectroscopy is dominated by the geometry of the atomic cluster rather than its electronic structure. Systematic errors linked to the (ε || heme_plane) polarized component give more problems in the extraction of the axial parameters of heme proteins in solution. As the majority of the signal in solution is due to the (ε || heme_plane) scattering, these errors affect the determination of the axial parameters thus limiting the accuracy of the XANES analysis of hemeproteins in solution.

Interestingly, the accuracy of the EXAFS determination to the Fe−heme displacement of the model system Fe(II)-TPPCl (measured with high S/N ratio) is higher than that measured by XANES (0.07 vs 0.15 Å), owing to the possibility to extract the contributing 4-body signal from a large data set including k-values up to 15 Å^{-1}, but vanishes when going to a more diluted system like Fe(II)Mb; on the other hand, the XANES accuracy remains substantially unaltered (0.15 vs 0.2 Å). Contrary to EXAFS, the XANES calculations are sensitive to the position of a water molecule located in the distal pocket of Fe(II)Mb, at a distance <4 Å from the iron center. The measured distance is 3.7 ± 0.2 Å, in agreement with the XRD value of 3.52 Å. This XANES sensitivity arises from the fact that far lighter atoms, at low photoelectron energies, have a much higher backscattering amplitude (about 0.75 at $R = 4$ Å and $k = 2$ Å^{-1}) than at higher energies (about 0.15 at $R = 4$ Å and $k = 9$ Å^{-1}).[49] Thus, the calculated induced variations of the XANES signal at energies <40 eV are well beyond the experimental noise. The C−N distance in Fe(III)MbCN is measured with 0.01 Å precision by EXAFS and 0.02 Å precision by XANES. Clearly, the accurate determination of the atomic distance of biatomic ligands such as NO, CO, and O_2 when bound to hemeproteins and heme-sensors is extremely important to shed light on their functional behavior.

In the present work we have used the Fe(III)MbCN sample to assess the sensitivity of the EXAFS and XANES fits to

(49) McKale, A. G.; Veal, B. W.; Paulikas, A. P.; Chan, S. K.; Knapp, G. S. *J. Am. Chem. Soc.* **1988**, *110*, 3763–3768.

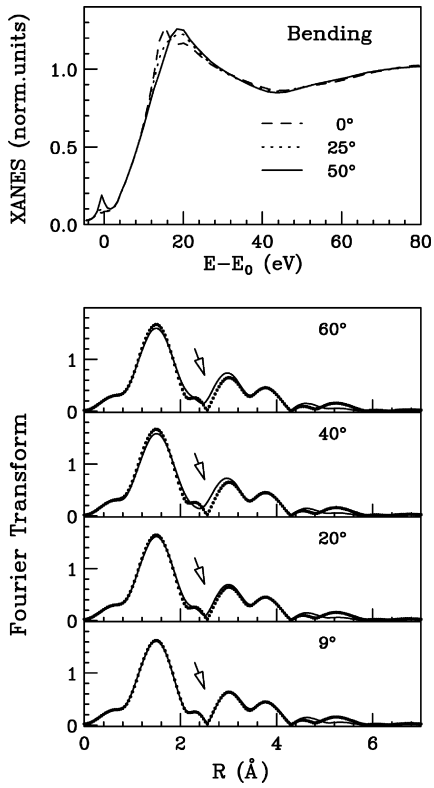

Figure 8. Sensitivity of XANES and FT-EXAFS calculations to the bending angle Fe−C−N.

the axial parameters, that is, the Fe−CN and Fe−N_{His} distances and the Fe−C−N bending angle. To this end we have fixed all of the other structural and nonstructural parameters, and we have calculated the spectra corresponding to different values of the selected structural parameter. The EXAFS and XANES sensitivity to the axial distances and the statistical correlation between these parameters and the Fe−Np distance is shown and discussed in the Supporting Information, Figures S1, S2, and S3.

Last, we examine the sensitivity of our MS EXAFS and XANES calculations toward the CN bending angle in Fe(III)MbCN. The FTs of the calculated GNXAS spectra with Fe−C−N angles of 9° (best fit, $\mathcal{R}$ value 0.796×10^{-6}), 20° ($\mathcal{R}$ value 0.857×10^{-6}), 40° ($\mathcal{R}$ value 0.112×10^{-5}), and 60° ($\mathcal{R}$ value 0.986×10^{-6}) are presented in Figure 8. Note that even if the quality of the fit becomes clearly poor for Fe−C−N angles higher than 20°, the sensitivity of the fit is not very high between 9° and 20°. Nevertheless, the difference of the $\mathcal{R}$ values obtained from different minimization procedures allows one to determine the Fe−C−N angle with an accuracy of ±6°. The sensitivity of the XANES spectra to the Fe−C−N angle can be deduced by looking at the changes occurring at the pre-edge and on the main XANES features (peaks **1**, **3**, and **4** of Figure 7). A similar behavior can be obtained for other biatomic ligands like CO, O_2, and NO (data not shown). In the past, interest in hemeprotein ligand binding research was mainly focused on peak **3**, proposed to be a marker of the bending angle, according to a small number of qualitative, heavy time-consuming, XANES calculations.[50] However, most of the computational limitations are overcome to date, and simulations can be carried out to explore significant portions of the parameter space, including all the relevant parameters. According to our extended calculations, peak **3** is affected not only by the bending angle but also strongly by the C−N distance and secondarily by the Fe−N_{His} and Fe−CN distances. Moreover, changes in the Fe−heme displacement still affect peak **3**, though this parameter is usually neglected in calculating hexa-coordinate low-spin heme-iron systems. Thus, too many parameters affect peak **3** to be a marker of the bending angle of biatomic molecules in hexa-coordinated heme-iron. On the contrary, Figure 8 shows a dramatic increase of the pre-edge peak **1**, associated with an increase of the bending angle to values bigger than 35°, that is not sensitive to other structural changes. According to our calculations feature **1** contains convoluted 1s→3d transitions to empty d-states of the ferric iron. Such transitions are dipole forbidden in the K-edge XANES spectra, but for a C_{4v} or C_{2v} local symmetry become partially allowed by p-d mixing. This case is different from that of the previously studied ferricyanate complexes for which, because of perfect octahedral symmetry, 1s-3d transitions are completely dipole forbidden and quadrupole transitions are thought to contribute to pre-edge features. Thus, an increase of d-p mixing seems reasonably related to the intensity enhancement of the pre-edge feature as the hybridization of iron d-states should involve not only the p-orbitals from iron itself and the carbon of CN but also those from the external nitrogen. A complete description of this effect would require bound-to-bound self-consistent field calculations, allowing one to extract, for each final molecular state, the contained fractions of atomic charges and orbitals from the Fe, C, and N atoms that are beyond the scope of this article. In particular, the intensity of the (ε || heme_normal) polarized, $1s \rightarrow [3d_{z^2} + \sigma(CN)]^*$ transition seems strongly increased by p-d mixing variations associated to lowering the local symmetry as in going from an upright to a bent configuration. Even if other determinants (mainly the electron density of d-states) can affect the intensity of the pre-edge peak **1**, we suggest that this feature, rather than peak **3**, could be related to bond angle changes between different ligand binding conformers when biatomic molecules act as sixth ligands to heme proteins.

The presence of multiple solutions, that is, different minima in the parameter space of the optimization procedure, is expected to occur, especially when the axial ligands of the iron have the same or similar atomic number, as the pyrrol nitrogens of the porphyrin plane. An example is shown in the upper panel of Figure 9. A double minimum was found during the MXAN best fitting procedure of Fe(III)MbH_2O. The two corresponding structures have well distinct values of axial and planar distances, the Fe−Np, Fe−N_{His} and Fe−O bond lenghts being 2.00, 2.16, and 2.16 Å versus 2.04, 2.00, and 2.28 Å, respectively, so that the calculated (ε || heme_normal) and (ε || heme_plane) polarized XANES spectra are strongly different. In spite of this, the unpolarized spectra, where axial and planar contribution are convoluted, are very similar. Note that no line-broadening is included in

(50) Bianconi, A.; Congiu-Castellano, A.; Durham, P. J.; Hasnain, S. S.; Phillips, S. *Nature* **1985**, *318*, 685–687.

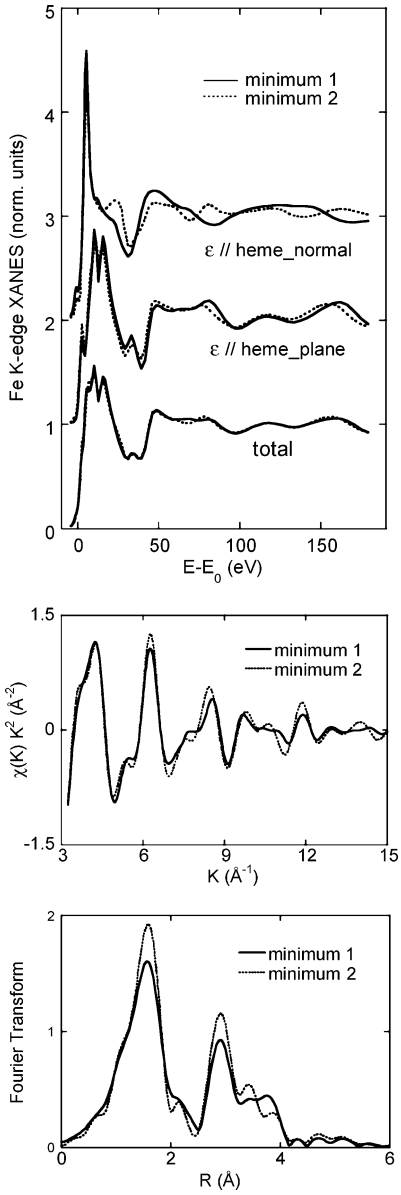

Figure 9. Double minimum found in the best fitting procedure for the unpolarized XANES spectrum of Fe(III)Fe(III)MbH$_2$O. The Fe−heme structure corresponding to minimum 1 has d(Fe−N$_p$) = 2.0 Å, d(Fe−N$_\varepsilon$) = 2.16 Å, d(Fe−O) = 2.16 Å. By contrast, the structure corresponding to minimum 2 has d(Fe−N$_p$) = 2.04 Å, d(Fe−N$_\varepsilon$) = 2.00 Å, d(Fe−O) = 2.28 Å. The calculated (without line-broadening) ε || heme_normal and ε || heme_plane polarized XANES spectra for these two structures (top and center curves) are strongly different, but the total unpolarized spectra (bottom curves) are very similar.

the calculations shown in Figure 9: differences become even smaller after including them. These two minima lead to almost identical fits of the experimental data (the fit due to the first minimum is shown in Figure 6, central curves); however, whereas the structural data corresponding to the first minimum are in excellent agreement with XRD and the EXAFS fit (Figure 4 central panel), those of the second minimum are not. Contrary to XANES, the EXAFS analysis is able in this case to discriminate between the two minima: the $\chi(k)$ and FT transformed theoretical signals corresponding to each of the two structures are compared in the lower panels of Figure 9. Note that sizable differences are visible in the energy region above 5 Å^{-1}, while only small differences are found in the low energy region, in agreement with the full MS XANES calculations. In particular there is a big difference in the amplitude of the first two peaks of the FT, (last panel of Figure 9) leading to a fit of the experimental data worse than that shown in Figure 4. Thus, in this case, the EXAFS analysis can solve a XANES ambiguity. However, in some cases multiple minima are a concern also for EXAFS that can be hopefully overcome by XANES. In the past we have already applied XANES to solve EXAFS ambiguities, such as its difficulty in establishing the metal coordination number[19] or in discriminating among backscatterers having close atomic numbers.[22] As a consequence there is a clear advantage in performing a combined XANES and EXAFS analysis to eliminate the ambiguities that are intrinsic to each technique.

Conclusion

XAS spectroscopy in solution recovers correct results for the structural parameters. Both XANES and EXAFS analyses are possible and their joint use is essential to avoid ambiguities linked to the existence of multiple minima. With the actual procedure, XANES data analysis of absolute spectra in solution provides the Fe−heme local structure with an accuracy of 0.02−0.03 Å on the Fe−Np distance, 0.05−0.07 Å on axial distances, 0.15−0.2 Å on Fe−heme displacement and about 20° on the bending angle, and 0.02 Å on the atomic distance of ligated biatomic molecules. This accuracy is approximately comparable to that of 1.4 Å resolution XRD on crystals. Use of more sophisticated models to describe atomic potential would be helpful to avoid systematic errors and achieve even better precision in XANES calculations. The reliability of this procedure demonstrates that XAS spectroscopy is a good tool to investigate ligand binding to hemes and hemeproteins. The combination of XANES and EXAFS with X-ray diffraction will be a valuable tool to obtain independent and complementary information on protein metal sites.

Acknowledgment. We acknowledge the European Synchrotron Radiation Facility for provision of synchrotron radiation facilities and the CASPUR computational center for providing the computational resources used in this work. We also thank Dr. Michael Borowski for assistance in using beamline BM29.

Supporting Information Available: EXAFS and XANES sensitivity to axial parameters, and Figures S1−S3. This material is available free of charge via the Internet at http://pubs.acs.org.

IC800982A